Int. J. Heat Mass Transfer. Vol. 35, No. 6, pp. 1407–1417, 1992
Printed in Great Britain

0017–9310/92 $5.00 + 0.00

Segmental heat transfer in a pin fin channel with ejection holes

S. C. LAU, R. D. McMILLIN and R. T. KUKREJA
Department of Mechanical Engineering, Texas A&M University, College Station, TX 77843-3123, U.S.A.

(*Received* 15 *October* 1990 *and in final form* 7 *June* 1991)

Abstract—An experimental investigation has been conducted to study, for turbulent air flow through a pin fin channel with ejection holes, the effects of varying the ejection hole configuration on the distribution of the regionally-averaged heat transfer and the overall pressure drop. The channel models the internal cooling passages near the trailing edges of rotor or stator blades in modern gas turbine engines. When air exits through ejection holes, the segmental heat transfer decreases much faster with increasing distance from the channel entrance and the overall channel pressure drop is lower than in the straight-flow-only case. Increasing the number of ejection holes and increasing the size of the ejection holes lower the distribution of the segmental heat transfer and the overall pressure drop.

INTRODUCTION

PIN FIN channels can be found in the blades of some modern gas turbine engines. Air from the engine compressor is forced to flow through an internal pin fin channel to cool the tail region of a blade. Some of the cooling air exits the pin fin channel through small ejection holes along the trailing edge of the blade and the rest through the blade tip. To maximize the efficiency of a gas turbine engine and to ensure its safe operation, a designer needs to have extensive knowledge of the heat transfer and friction characteristics of flow through such pin fin channels.

Turbulent heat transfer in pin fin channels has been studied by a number of researchers, for instance, Brown *et al.* [1], VanFossen [2], Brigham and VanFossen [3], Metzger and Haley [4], Metzger *et al.* [5, 6], and Lau *et al.* [7]. Lau *et al.* [8, 9] conducted experiments to demonstrate that, when there was flow exiting a pin fin channel through ejection holes, the gradually decreasing mass flow in the channel and the turning of the air stream in the channel affected significantly the overall heat transfer from the pin fin channel. They presented overall heat transfer and pressure drop results for various channel and ejection hole/slot geometries, and a wide range of Reynolds numbers.

The objective of the present investigation is to study the effects of varying the configuration of the ejection holes and the flow rate on the regionally-averaged heat transfer distribution for the flow of cooling air through pin fin channels in turbine blades. The pin fin cooling passages are modeled as a rectangular pin fin channel of eight segments with ejection holes in one of the side walls. The straight-flow exit of the channel is either wide open or blocked. The distribution of the segmental heat transfer coefficient and the overall pressure drop across the pin fin channel are obtained for various ejection hole configurations and for a range of Reynolds numbers typical of air flow in pin fin cooling passages in turbine blades.

EXPERIMENTAL APPARATUS

The test section for the present experimental investigation is an 8.75 : 1 rectangular channel with a flow cross-section of 55.6 mm (2.19 in.) by 6.35 mm (0.25 in.). Thirty-two rows of three short pins 6.35 mm (0.25 in.) in diameter are staggered in the channel with spacings of 13.7 mm (0.541 in.) and 15.9 mm (0.625 in.) in the straight-flow and the ejection-flow directions, respectively. Therefore, $H/D = 1.0$, $X/D = 2.165$, $S/D = 2.50$, and lines joining the centers of the pins form an array of equilateral triangles.

The test section consists of eight identical segments (Fig. 1). The top and bottom walls of each segment are 6.35 mm (0.25 in.) thick aluminum plates that measure 54.2 mm (2.135 in.) long and 61.9 mm (2.438 in.) wide. The pins are 19.1 mm (0.75 in.) long aluminum rods and are pressed into a staggered array of holes in the two principal walls. The eight segments are joined together end to end with silicone rubber adhesive. A 0.76 mm (0.030 in.) thick rubber gasket serves to minimize heat conduction between adjacent segments. Thus, the total length of the test section is 0.44 m (17.32 in.).

The two side walls of the test channel are machined from acrylic rectangular bars. Each has a 6.35 mm (0.25 in.) by 3.18 mm (0.125 in.) longitudinal rib that serves to align the eight aluminum segments. One of the side walls is 6.35 mm (0.25 in.) thick and 19.05 mm (0.75 in.) high and is attached to the aluminum segments permanently with small cap screws and silicone rubber adhesive. The other side wall is 25.4 mm (1.0 in.) thick and 19.05 mm (0.75 in.) high and is attached to the test channel segments with silicone rubber adhesive only.

NOMENCLATURE

A	total heat transfer area, including all aluminum surfaces exposed to air flow in a channel segment [m^2]
A_{min}	area of minimum flow cross-section in pin fin channel [m^2]
c_p	specific heat of air at average bulk temperature [J kg^{-1} K^{-1}]
d	diameter of ejection holes [m]
D	diameter of pins [m]
f	overall friction factor, equation (4)
H	height of pins [m]
k	thermal conductivity of air at average bulk temperature [W m^{-1} K^{-1}]
L	length of ejection holes [m]
$\dot{m}$	total mass flow rate of air [kg s^{-1}]
n	segment number, $n = 1$ and 8 for the first and the last channel segments from the channel entrance, respectively
N	number of pin rows in test channel, $N = 32$
$\overline{Nu}_D$	segmental Nusselt number in straight-flow-only case, equation (1)
$\overline{Nu}_{D1}$	segmental Nusselt number based on T_{bi} in ejection-flow cases, equation (5)
$\overline{Nu}_{D2}$	segmental Nusselt number based on $\bar{T}_b$ in ejection-flow cases, equation (6)
$\overline{Nu}_{D3}$	segmental Nusselt number based on $\bar{T}_j$ in ejection-flow cases, equation (7)
Δp_{total}	overall pressure drop across test channel [N m^{-2}]
$\dot{q}_{cond}$	net rate of heat gain by conduction for a channel segment [W]
$\dot{q}_{in}$	power input to a channel segment [W]
$\dot{q}_{loss}$	rate of heat loss through insulation from a channel segment [W]
$\dot{q}_{net}$	net rate of heat transfer from a channel segment to flowing air [W]
Re_D	Reynolds number, equation (3)
S	pin spacing in ejection-flow direction [m]
$\bar{T}_b$	average bulk temperature of air in a channel segment [K]
T_{bi}	bulk temperature of air at test channel inlet [K]
$T_{bi,i}$	bulk temperature of air at inlet of a channel segment [K]
T_{bo}	bulk temperature of air at straight-flow exit of test channel [K]
$T_{bo,i}$	bulk temperature of air at straight-flow exit of a channel segment [K], equation (2)
$\bar{T}_j$	average temperature of ejection airstream for a channel segment [K]
$\bar{T}_w$	average wall temperature for a channel segment [K]
u_{max}	velocity of air at minimum flow cross-section in test channel [m s^{-1}]
x	distance from channel entrance in straight-flow direction [m]
X	pin spacing in straight-flow direction [m].

Greek symbols

μ	dynamic viscosity of air at average bulk temperature [N s m^{-2}]
ρ	density of air at average bulk temperature [kg m^{-3}].

For each set of experiments with ejection flow, the thicker of the two side walls is replaced with a side wall that has an array of 63, 32 or 16 equally-spaced ejection holes. These ejection holes are 3.18 mm (0.125 in.) or 6.35 mm (0.25 in.) in diameter and their centers are located half-way between the top and the bottom walls. In the 32 ejection-hole case, the center of each hole is aligned with the centers of the three pins in a pin row. Since the length of the ejection holes is also the sum of the thickness of the side wall and the height of the longitudinal rib, the length-to-diameter ratio of the ejection holes, L/d, is either 4.5 or 9.0. Table 1 gives the configurations of the ejection holes in all of the cases studied. In two of the cases, the straight-flow exit of the test channel is blocked to force all of the cooling air to flow through the ejection holes. Figure

Table 1. Ejection hole configurations

Test case	Ejection hole diameter (mm/in.)	Ejection hole length-to-diameter ratio	Exit configuration	
			Straight-flow exit	Ejection-flow exit
1	—	—	Open	—
2a	3.18/0.125	9.0	Open	63 holes
2b	3.18/0.125	9.0	Blocked	63 holes
3a	3.18/0.125	9.0	Open	32 holes
3b	3.18/0.125	9.0	Blocked	32 holes
4	3.18/0.125	9.0	Open	16 holes
5	6.35/0.250	4.5	Open	32 holes
6	6.35/0.250	4.5	Open	16 holes

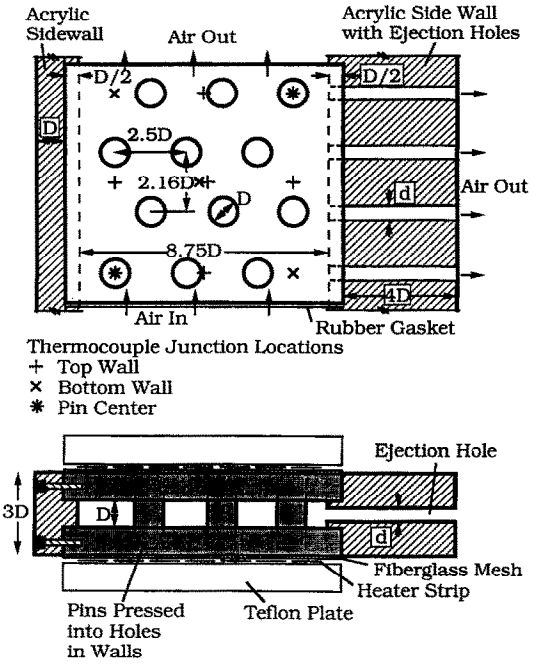

FIG. 1. Schematic of a channel segment.

2 shows the test channel with three typical ejection hole configurations.

Each of the top and bottom walls of the test channel is heated uniformly by passing electrical current through seven parallel, longitudinal strips of 0.025 mm (0.001 in.) thick stainless steel foil (see Fig. 1).

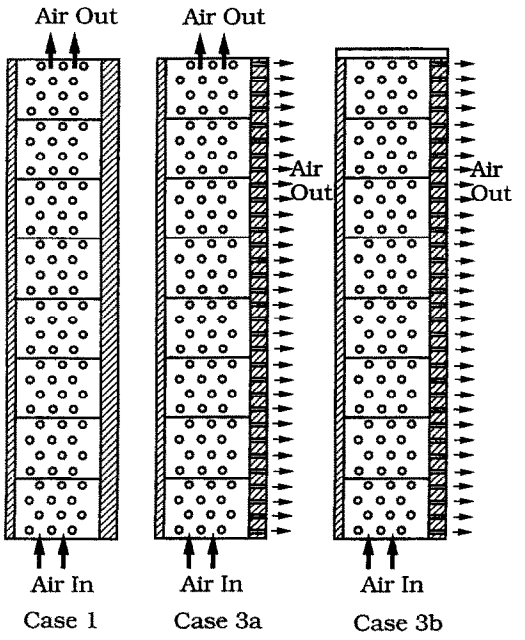

FIG. 2. Schematic of test channel with three typical ejection hole configurations.

Each strip is 6.35 mm (0.25 in.) wide and adjacent strips are separated from each other by a 1.59 mm (0.0625 in.) wide gap. The strips are sandwiched between the exterior surface of each channel wall and a 6.35 mm (0.25 in.) thick Teflon plate. Silicone rubber adhesive holds the heater strips onto the Teflon plate. A fine-grid fiberglass mesh and silicone rubber adhesive insulate the strips electrically from the aluminum wall. The strips are connected in series electrically with bus bars attached to the two ends of the Teflon plate with small screws.

The test section is fabricated with precision. All of its dimensions are accurate to within ± 0.05 mm (± 0.002 in.).

During an experiment, clean, dry air is supplied from a building compressor. Before entering the test section, the air passes through a storage tank, a drier, a flow regulator, two control valves, an orifice flow meter, a settling chamber, and an entrance section (Fig. 3). Air exits the test flow loop into the air-conditioned laboratory.

The entrance section is constructed of 12.7 mm (0.50 in.) thick acrylic plates. It has the same flow cross-section as that of the test channel and is 25.4 cm (10.0 in.) long to ensure that the flow is hydrodynamically fully developed at the inlet of the test channel. The upstream end of the entrance channel is attached permanently to the settling chamber with acrylic glue.

The downstream end of the entrance channel is mated to the upstream end of the test channel with two acrylic flanges that are held together with six bolts. The two flanges are attached permanently to the downstream end of the entrance channel and the upstream end of the test channel, respectively, with epoxy and small flat-head machine screws. An O-ring gasket and vacuum grease prevent air leakage between the flanges during an experiment.

The downstream half of the entrance section and the test section are insulated with at least four inches of fiberglass and Styrofoam insulation on all sides. At the straight-flow and ejection-flow exits, the Styrofoam insulation is cut to provide two short diverging channels for the air to leave the test section and for

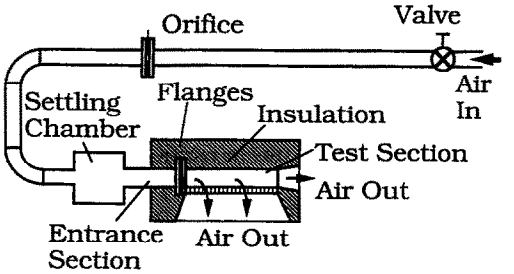

FIG. 3. Schematic of test flow loop.

maintaining the test channel exits at atmospheric pressure.

INSTRUMENTATION

The wall temperatures are measured with 80 30-gage copper–constantan thermocouples with Teflon insulation—ten thermocouples for each channel segment (see Fig. 1). The thermocouple junctions are installed in small deep holes that are drilled into the top and bottom walls of each segment or drilled into the pins. To ensure good contact between each thermocouple junction and a channel wall or a pin, the thermocouple is held in place with epoxy in a shallow groove on the outside surface of the wall, forcing the thermocouple junction against the bottom of the hole. The bottom portion of the hole is then filled with a silver-based paint. After the paint dries, the top of the hole and the groove are filled with epoxy to hold the thermocouple wire securely in place. An ohmmeter is used to check for good contact between the thermocouple junction and the channel wall or the pin.

The inlet air temperature is measured with two thermocouples whose junctions protrude into the airstream in the entrance section. The temperatures of the air at the straight-flow exit and at the ejection holes are measured with a thermocouple probe. The temperatures on the outside surface of one of the Teflon heater-strip support plates are measured with eight thermocouples—one at each test section segment. The temperature on the outside surface of the insulation is measured with two thermocouples. The temperatures on the Teflon plate and on the outside surface of the insulation are for the estimation of heat loss through the insulation during an experiment.

The outputs of all 93 thermocouples are recorded with a data logger. With the thermocouple probe, many more additional air temperature readings (up to 63 ejection-flow temperature readings and ten straight-exit-flow temperature readings) are recorded.

The total power input to the heater strips is controlled with a variable transformer. The voltage drop across the heater strips and the current through the heater strips are measured with two $5\frac{1}{2}$-digit TRMS multimeters.

The rate of mass flow through the test section is measured with a calibrated 6.35 cm (2.5 in.) orifice flow meter with a 45°-tapered, 2.54 cm (1.0 in.) orifice and flange taps. The pressure drop across the orifice and the pressure upstream of the orifice with respect to the atmospheric pressure are measured with an oil manometer and a mercury manometer, respectively.

Sixteen static pressure taps are installed along the acrylic side wall with no ejection hole, which is attached to the channel segments permanently. An additional static pressure tap is installed in the top wall of the entrance section near the test section inlet. The overall pressure drop across the test section and the local pressures with respect to the atmospheric pressure are measured with one of several oil or mercury manometers, or a micromanometer, depending on the measurement range.

EXPERIMENTAL PROCEDURE

For each ejection hole configuration studied, at least six experiments are conducted with the Reynolds number ranging between 6000 and 40 000. Before initiating each set of experiments, the test apparatus is checked for possible air leakage (with a solution of soap and water), consistency of the total electrical resistance of the heater strips, and continuity of all thermocouple wires.

A typical experiment lasts 3 h. After compressed air is allowed to flow through the test section at a predetermined rate, electrical current is passed through the heater strips. Power input to the heater strips is set to maintain a desired difference between the temperature of the inlet air and the average wall temperature at the last channel segment. The system attains a steady state in about 2 h. During that time, the pressure drop across the orifice is monitored periodically and the flow regulator (or one of the control valves) is adjusted whenever it is necessary to maintain the air flow rate constant. The power input to the heater strips is raised or lowered whenever the last channel segment attains a temperature lower than or higher than the desired temperature.

After the system attains a steady state, the atmospheric pressure, the pressure drop across the orifice, the gage pressures upstream of the orifice and at the taps on the test section are recorded. A printout of all the thermocouple readings is then obtained and the power input to the heaters recorded. Ten sample temperatures of the air at the straight-flow exit are recorded with the tip of the thermocouple probe (that is, the thermocouple junction) positioned near the straight-flow exit of the test channel. In the straight-flow-only case, the average of the temperatures is used to check the calculated air bulk temperature at the straight-flow exit.

In the cases with ejection flow, the temperature of the air at the exit of each ejection hole is measured with the tip of the thermocouple probe positioned just outside the ejection hole. Because of the relatively small size of the ejection hole and the acrylic side wall, the temperature does not vary significantly in the ejection airstream and only one reading of the temperature at each ejection hole is recorded.

In a calibration experiment, the inlet air temperature is measured with the two thermocouples whose junctions protrude into the airstream in the entrance section while the air flow rate is raised and lowered alternately within a range corresponding to $6000 < Re_D < 40\,000$. Since there is no measurable variation in the indicated inlet air temperature when the air flow rate is varied between the flow rate limits, the indicated temperature gives the static or true temperature of the inlet airstream.

REDUCTION OF DATA

In the straight-flow-only case (case 1), the regionally-averaged Nusselt number for each channel segment, or the segmental Nusselt number, is calculated from

$$\overline{Nu}_D = \left\{\frac{(\dot{q}_{net}/A)}{(\bar{T}_w - \bar{T}_b)}\right\}\left(\frac{D}{k}\right) = \left\{\frac{[(\dot{q}_{in} - \dot{q}_{loss} + \dot{q}_{cond})/A]}{(\bar{T}_w - \bar{T}_b)}\right\}\left(\frac{D}{k}\right). \quad (1)$$

The rate of heat input, $\dot{q}_{in}$, is the total power input to the heater strips (the product of the measured voltage drop across the heater strips and the current through the strips) divided by eight. The rate of heat loss through the fiberglass and Styrofoam insulation, $\dot{q}_{loss}$, is calculated with the measured temperatures on the outside surface of one of the Teflon heater-support plates and on the outside surface of the insulation, assuming one-dimensional heat conduction in the insulation.

The rate of net heat gain by conduction along the channel walls in the straight-flow direction, $\dot{q}_{cond}$, is the difference between the rate of heat conduction from the channel segment immediately downstream and the rate of heat conduction to the segment immediately upstream. The calculation of heat conduction between adjacent segments assumes one-dimensional heat conduction, uses the average of the three wall temperatures nearest the rubber gaskets in each segment, and takes into account the thermal resistances in series associated with the aluminum walls and the rubber gaskets.

The total heat transfer area, A, includes the exposed surface areas of the top wall, the bottom wall, and the pins, but not the side walls. The average wall temperature is the average of the ten measured wall temperatures for each segment. The average bulk temperature is the average of the local bulk temperatures at the inlet and exit of the segment, $T_{bi,i}$ and $T_{bo,i}$. The exit bulk temperature is calculated from the inlet bulk temperature based on an energy balance:

$$T_{bo,i} = T_{bi,i} + \frac{\dot{q}_{net}}{\dot{m}c_p}. \quad (2)$$

For all straight-flow-only test runs, the calculated bulk temperature at the exit of the test channel, T_{bo} (that is, at the exit of the last segment), is comparable to the average of the ten measured air temperature samples at the exit.

The Reynolds number is defined in terms of the pin diameter and the air velocity at the minimum flow cross-section in the pin fin channel:

$$Re_D = \frac{\rho u_{max} D}{\mu} = \frac{\dot{m} D}{A_{min}\mu}. \quad (3)$$

The total pressure drop across the test section and the local pressures in the test section with respect to the atmospheric pressure are normalized by the dynamic pressure based on u_{max}. The former is defined as the overall friction factor. Thus

$$f = \frac{\Delta p_{total}}{\frac{1}{2}\rho u_{max}^2 N} = \frac{2\Delta p_{total}\rho}{N}\left(\frac{A_{min}}{\dot{m}}\right)^2 \quad (4)$$

where $N = 32$ is the number of pin rows in the test section.

In all of the above equations, the properties of the flowing air are evaluated at the average of the bulk temperatures at the inlet and the exit of the test channel.

In all cases with ejection flow, the rate of mass flow in the test channel decreases with increasing distance from the channel entrance. The flowing air turns in the channel to exit through the ejection holes. Since the rate of mass flow through each segment decreases and its variation is not known, an average bulk temperature for each segment cannot be determined based on an energy balance. Three Nusselt numbers are defined as follows:

$$\overline{Nu}_{D1} = \left\{\frac{(\dot{q}_{net}/A)}{(\bar{T}_w - T_{bi})}\right\}\left(\frac{D}{k}\right) \quad (5)$$

$$\overline{Nu}_{D2} = \left\{\frac{(\dot{q}_{net}/A)}{(\bar{T}_w - \bar{T}_b)}\right\}\left(\frac{D}{k}\right) \quad (6)$$

$$\overline{Nu}_{D3} = \left\{\frac{(\dot{q}_{net}/A)}{(\bar{T}_w - \bar{T}_j)}\right\}\left(\frac{D}{k}\right). \quad (7)$$

In equation (5), the segmental Nusselt number is defined in terms of the difference between the average wall temperature and the bulk temperature of the air entering the test channel. The segmental Nusselt number in equation (6) is in terms of an average bulk temperature that is calculated with the assumption that the rate of mass flow through the test channel is constant. The segmental Nusselt number in equation (7) is based on the average of the measured temperatures of the air flow through ejection holes at a channel segment.

In the ejection-flow cases, the Reynolds number and the total pressure drop are both based on the rate of total mass flow at the channel entrance as given in equations (3) and (4). The properties of the flowing air are evaluated at the average of the bulk temperatures at the inlet and the straight-flow exit of the test channel. In the cases with a blocked straight-flow exit, the properties of the flowing air are evaluated at the average of the bulk temperature at the inlet and the temperature of the airstream at the last ejection hole.

EXPERIMENTAL UNCERTAINTIES

The factory-calibrated orifice flow meter is rated at $\pm 1.0\%$ accuracy. The largest variation of the pressure drop across the orifice, which occurs during low

Reynolds number ($Re_D \approx 6000$) runs, is never more than $\pm 5\%$. Even if the uncertainty of the measured pressure drop across the orifice is conservatively estimated to be $\pm 5\%$, the uncertainty of the rate of total mass flow through the test section is less than $\pm 3.5\%$. Based on the tolerance of 0.05 mm (0.002 in.) for all the dimensions of the test section, the uncertainties of A_{min} and D are estimated to be ± 1.3 and $\pm 0.8\%$, respectively. Using equation (3), an estimated uncertainty of $\pm 2.0\%$ for the dynamic viscosity of air, and the uncertainty estimation method of Kline and McClintock [10], the maximum uncertainty of the calculated Reynolds number is $\pm 4.3\%$.

The percentage variations of the voltage drop across the heater strips and the current through the heat strips are negligibly small for all experiments. The power input to a channel segment, however, may deviate from one-eighth of the total power input due to the small non-uniformity of the cross-sections of the heater strips. Errors may also be introduced when the rate of heat loss through the insulation is estimated assuming one-dimensional heat conduction, although the rate of heat loss through the insulation is at most 8.0% of the power input for a channel segment. Heat conduction along the wall is relatively small except when there is a large temperature difference between two adjacent segments. The net heat gain or loss by conduction is significant at the first and the last segments.

The uncertainty of the rate of net heat transfer to the airstream in a channel segment is estimated to be about $\pm 5.0\%$. Using a conservatively estimated uncertainty of $\pm 5.0\%$ for the wall/air temperature differences results in an uncertainty of $\pm 7.5\%$ in the calculated segmental Nusselt numbers.

Similarly, with a maximum variation of the overall pressure drop of $\pm 3\%$ during an experiment, the normalized overall pressure drop has an uncertainty of $\pm 6.4\%$.

PRESENTATION OF RESULTS

Heat transfer results—straight-flow case

In Fig. 4, the segmental Nusselt number distributions for straight flow through the test channel (case 1) are given. The data are based on 15 test runs with $Re_D = 5955$, 6190, 6224, 8732, 8908, 12 949, 13 079, 19 118, 19 505, 20 341, 30 368, 30 483, 40 552, 40 604, and 40 689. A different total power input is used in each of the test runs with approximately the same Reynolds number. The total power input in a test run may be as high as twice that in another test run at approximately the same Reynolds number. Since the results show that Nu_D as a function of Re_D and x/X is independent of the total power input, Nu_D is plotted versus x/X for six nominal values of Re_D only in Fig. 4.

Figure 4 shows that the segmental Nusselt number decreases slightly with increasing distance from the channel entrance. The data for the 15 test runs fall on six well-spaced straight lines corresponding to the six nominal Reynolds numbers. For $Re_D \approx 6000$, the value of Nu_D of the last channel segment is about 17.3% lower than that of the first segment. For $Re_D \approx 40\,000$, the decrease is about 7.3%. The trends of the results are consistent with those for straight flow through pin fin channels in published work [5]. The reported initial increase in the row-averaged Nusselt number over the first two to four pin rows is not observed, however, since the Nusselt number is averaged over each segment with four pin rows in this study.

In Fig. 5, the variations of the segmental Nusselt number for the first and the last channel segments with the Reynolds number are given on a log–log plot. The data fall on two slightly converging straight lines. In Fig. 5, the overall average Nusselt number–Reynolds number results from Metzger and Haley [4] and Lau *et al.* [9] are also shown. The results of the present investigation compare very well with those from the previous studies, considering that the test section geometries and test conditions (pin spacings, channel aspect ratio, channel length, etc.) are quite different in the three studies.

Since Nu_D for the first and the last channel segments can be expressed as power functions of Re_D, least squares curve fit straight lines are obtained and are shown in Fig. 5. The equations for the two lines are

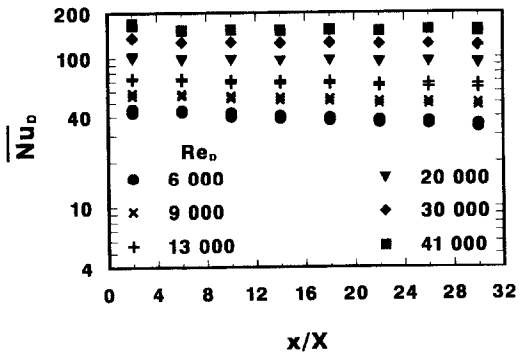

FIG. 4. Distributions of segmental Nusselt number, case 1—straight flow only.

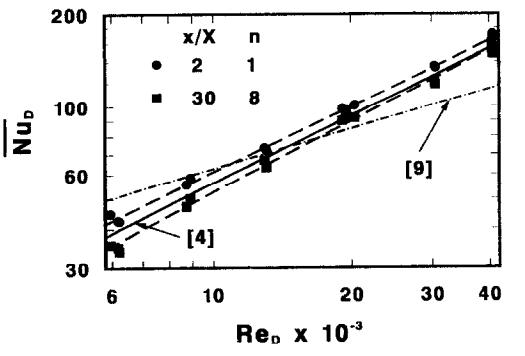

FIG. 5. Nu_D as a function of Re_D for first and last channel segments, case 1—straight flow only.

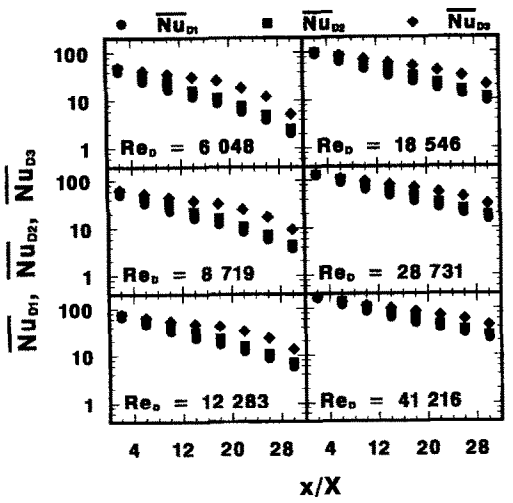

FIG. 6. Segmental Nusselt number distributions, case 2a.

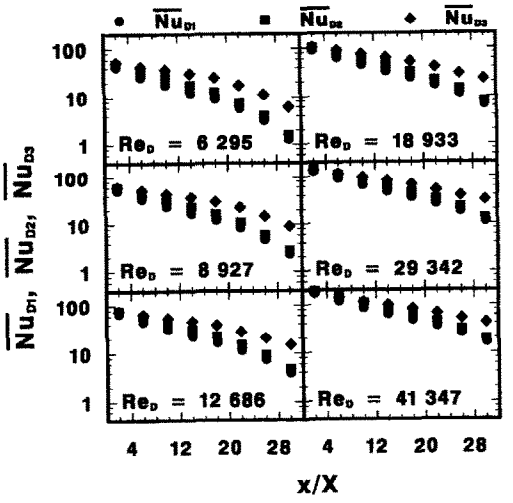

FIG. 7. Segmental Nusselt number distributions, case 2b.

$$(\overline{Nu}_D)_{n=1} = 0.0893 Re_D^{0.709}$$
$$(\overline{Nu}_D)_{n=8} = 0.0438 Re_D^{0.770} \quad (8)$$

where n is the segment number, with $n = 1$ and 8 for the first and the last segments from the channel entrance, respectively. It can be shown that all $\overline{Nu}_D$ data can be correlated as follows:

$$\frac{\overline{Nu}_D}{(\overline{Nu}_D)_{n=1}} = \left\{\frac{(\overline{Nu}_D)_{n=8}}{(\overline{Nu}_D)_{n=1}}\right\}^{(n-1)/7}. \quad (9)$$

Combining equations (8) and (9) results in the following equation that can be used to predict $\overline{Nu}_D$ for a given channel segment as a function of Re_D:

$$\overline{Nu}_D = 0.0989(0.903)^n Re_D^{(0.701+0.00859n)}. \quad (10)$$

Equation (10) correlates the $\overline{Nu}_D$ data from all 15 straight-flow-only test runs with a maximum deviation of 8.3% (deviation based on the average of the corresponding experimentally-determined and predicted values). Ninety-three percent of the $\overline{Nu}_D$ data are within $\pm 5.7\%$ of the corresponding value of $\overline{Nu}_D$ predicted with equation (10) and 98% of the $\overline{Nu}_D$ data are within $\pm 6.4\%$.

Heat transfer results—ejection-flow cases

Figures 6–12 present the distributions of the three segmental Nusselt numbers defined in equations (5)–(7) for the various ejection-flow cases. In each of the figures, $\overline{Nu}_{D1}$, $\overline{Nu}_{D2}$ and $\overline{Nu}_{D3}$ are plotted as functions of x/X for six Reynolds numbers: $Re_D \approx 6000$, 9000, 12 000, 19 000, 30 000, and 40 000. The three Nusselt numbers are defined, respectively, in terms of the inlet bulk temperature, the average of the bulk temperatures at the inlet and straight-flow exit of each channel segment assuming constant mass flow rate (that is, no ejection flow), and the average of the air temperatures at the ejection-hole exits at each channel segment.

With some of the air flow inside each channel segment turning to exit through the ejection holes, there

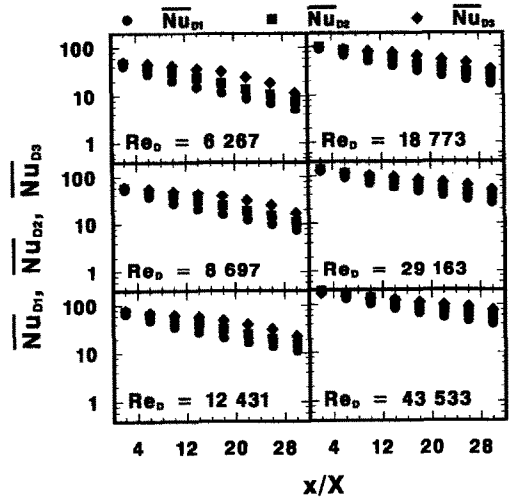

FIG. 8. Segmental Nusselt number distributions, case 3a.

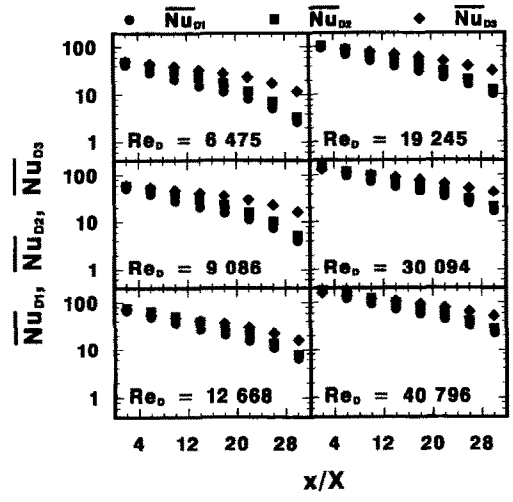

FIG. 9. Segmental Nusselt number distributions, case 3b.

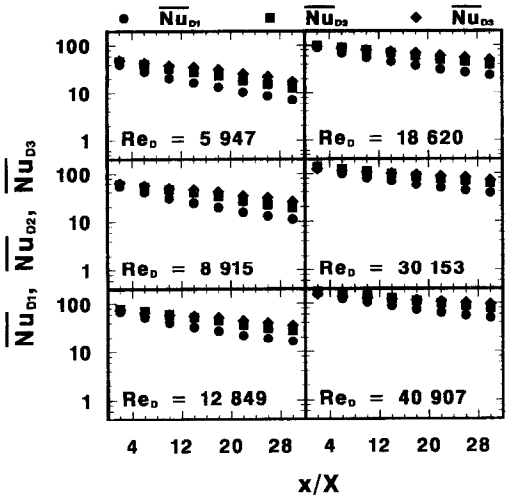

FIG. 10. Segmental Nusselt number distributions, case 4.

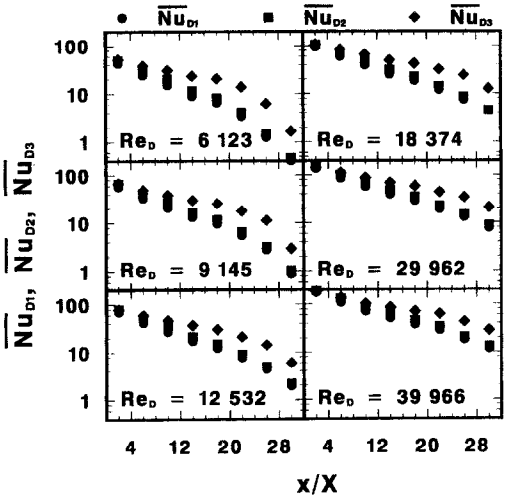

FIG. 11. Segmental Nusselt number distributions, case 5.

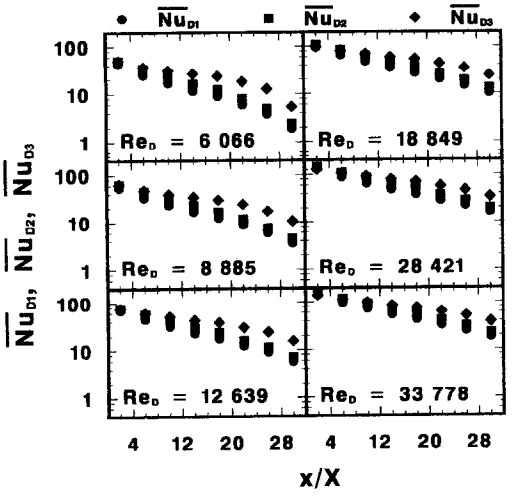

FIG. 12. Segmental Nusselt number distributions, case 6.

are significant variations of the temperature, velocity, and rate of mass flow of the air in both the straight-flow and ejection-flow directions (in addition to the variations of these parameters as a result of the air flowing around the pin fins). An average bulk temperature for each channel segment cannot be accurately predicted without detailed data on the local distributions of the air temperature and velocity in a channel segment and at the ejection holes.

Figures 6–12 show that all three segmental Nusselt numbers decrease with increasing x/X. For a given Re_D, the $\overline{Nu}_{D3}$ distribution is always higher than the $\overline{Nu}_{D2}$ distribution, which, in turn, is always higher than the $\overline{Nu}_{D1}$ distribution. The difference among the three Nusselt number distributions is due to the use of different reference bulk temperatures in defining the three Nusselt numbers. It will be shown shortly that, at any given x/X, the measured air temperature at an ejection hole exit is always higher than the bulk temperature that is calculated assuming no ejection flow. Obviously, the latter bulk temperature should always be higher than the inlet bulk temperature.

In each of the ejection-flow cases, the Nusselt number distributions are higher for larger values of the Reynolds number. The Nusselt numbers at the first channel segment are generally about the same as that for straight flow with the same Reynolds number. However, the distributions in the ejection-flow cases drop with increasing x/X much faster than those in the straight-flow cases, especially when the Reynolds number is small. In case 2a, $\overline{Nu}_{D2}$ decreases by 94.5, 88.2, and 84.7% between the first channel segment and the last channel segment for Re_D = 6048, 18 546, and 41 216, respectively. The percentage decrease in any of the Nusselt numbers with increasing x/X is always larger at lower Reynolds numbers.

The decrease in the Nusselt number distributions with increasing distance from the channel entrance is the result of the gradual decrease of the mass flow in the channel as air exits through the ejection holes. When the Reynolds number is large, the inertia of the flowing air pushes more air further downstream in the straight-flow direction, resulting in a generally smaller drop in the Nusselt numbers. It is interesting to note that there is a larger drop in the local static pressure (relative to the atmospheric pressure and non-dimensionalized with respect to the dynamic pressure based on u_{max}) in the pin fin channel with increasing x/X near the channel entrance when Re_D is small than when Re_D is large. The larger relative pressure drop indicates that a larger portion of flowing air exits the channel through the ejection holes near the channel entrance when Re_D is small.

Blocking the straight-flow exit does not significantly affect the Nusselt numbers at the channel segments near the channel entrance but lowers the Nusselt numbers at the downstream channel segments (see Figs. 6–9). The Nusselt numbers at the last three channel segments in the ejection-flow cases with a blocked straight-flow exit (cases 2b and 3b) generally drop

faster with increasing x/X than those in corresponding cases with an open straight-flow exit (cases 2a and 3a).

With a blocked straight-flow exit, all of the air is forced to exit through the ejection holes. The local pressure near a blocked straight-flow exit is higher than that near an open straight-flow exit. The higher local pressure in the pin fin channel forces more air to exit the ejection holes and leaves less air to cool the pin fin channel. In the open straight-flow exit cases, the local pressure near the channel exit is almost the same as the atmospheric pressure. As a result of the small pressure drop across the ejection holes near the channel exit, there is almost no air flowing through the last several ejection holes.

Comparing Figs. 6, 8, and 10 reveals that there is a smaller drop in the Nusselt numbers with increasing x/X as the number of ejection holes is decreased. Finally, comparing the Nusselt numbers in the corresponding cases with 3.18 mm (0.125 in.) and 6.35 mm (0.25 in.) ejection holes (Figs. 8 and 10–12) shows that the drop in the Nusselt numbers with increasing x/X is much larger in the cases with larger ejection holes. The segmental Nusselt number distributions are strongly dependent on the rate of mass flow in the pin fin channel. With a larger number of ejection holes or an increase in the size of the ejection holes, there is less resistance for the cooling air to exit through the ejection holes, resulting in a larger drop in the air mass flow rate in the pin fin channel and less effective cooling of the channel.

Overall pressure drop

Figure 13 gives the overall pressure drop for the straight-flow-only case and the various ejection-flow cases studied. The overall friction factor, defined in equation (4), is plotted as a function of Re_D in a log–log plot. The results in all cases fall on straight lines with small negative slopes—that is, f decreases slightly with increasing Re_D and f is a power function of Re_D.

The overall pressure drop across the pin fin channel is by far the largest in the straight-flow-only case, with the value of f ranging from 0.36 to 0.25. The results for the ejection-flow cases show that increasing the number of ejection holes or the size of the holes reduces the overall channel pressure drop. Blocking the straight-flow exit (in cases 2b and 3b), however, increases the overall channel pressure drop slightly.

Temperature distributions

In Fig. 14, sample wall and bulk temperature distributions are shown for four test runs:

(a) in the straight-flow-only case (case 1, $Re_D = 19\,118$);

(b) in the case with ejection flow through 63 3.18 mm (0.125 in.) holes and an open straight-flow exit (case 2a, $Re_D = 28\,880$);

(c) in the case with ejection flow through 63 3.18 mm (0.125 in.) holes and a blocked straight-flow exit (case 2b, $Re_D = 29\,342$); and

(d) in the case with ejection flow through 32 3.18 mm (0.125 in.) holes and an open straight-flow exit (case 3a, $Re_D = 18\,773$).

The average of the ten measured temperatures in the walls of each of the eight channel segments is given along with the largest and the smallest of the measured temperatures. The bulk temperature at the straight-flow exit of each channel segment is calculated with equation (2).

In the cases with ejection flow, the bulk temperature distribution is obtained by setting the mass flow rate in the test channel constant, that is, by assuming no mass flow through the ejection holes. Therefore, the calculated bulk temperatures in the ejection-flow cases are not the actual mean temperatures of air at the straight-flow exits of the channel segments.

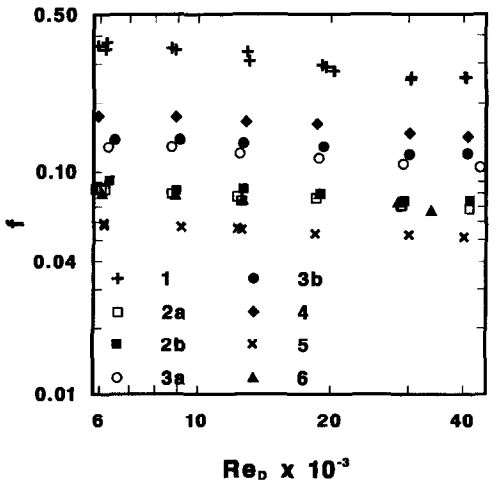

FIG. 13. Overall friction factor, all cases.

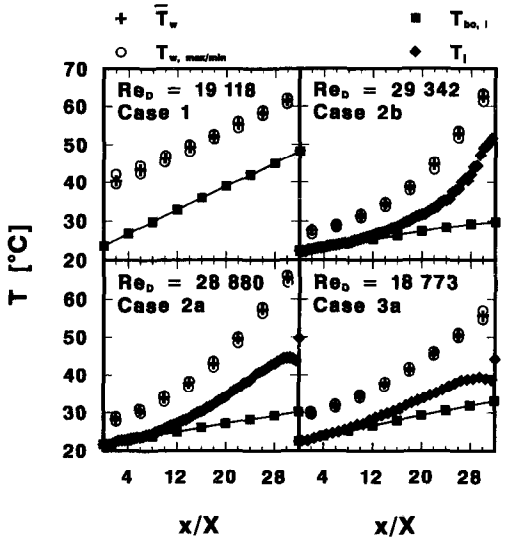

FIG. 14. Sample wall and air temperature distributions.

Figure 14 shows that, in the straight-flow-only case, both the average wall temperature and the bulk temperature increase linearly with increasing distance from the channel entrance. In a given channel segment, the local wall temperature is slightly lower at an upstream measurement station than at a downstream station, and the temperatures in the pins are generally lower than those in the walls. The variation of the values of the ten wall temperatures in a channel segment, however, is relatively small compared to the average wall temperature–bulk temperature difference.

The bulk temperature distribution is not exactly a straight line since the net heat input to the flowing air varies slightly from segment to segment. Although the average wall temperature and bulk temperature distributions shown appear to have the same slope, the two distributions diverge slightly with increasing x/X for most test runs.

The average of the measured air temperatures at the channel exit compares very well with the calculated exit bulk temperature. In all straight-flow-only runs, the average of the measured temperatures of the exiting air is slightly higher than the calculated exit bulk temperature. The average of the measured air temperatures at the channel exit is not used in any calculation since it is not the exact exit bulk temperature.

In the ejection-flow cases, the slope of the average wall temperature distribution increases with increasing distance from the channel entrance. With approximately the same amount of heat input to the airstream from each channel segment, the high average wall temperature near the straight-flow exit indicates that the channel walls are cooled less effectively there. This is the result of the decreasing air flow rate in the straight-flow direction, as air exits the channel through the ejection holes.

The measured air temperature at the exit of an ejection hole generally increases with increasing x/X. The ejection airstream temperature distribution deviates from the average wall temperature distribution more when the straight-flow exit is open than when it is blocked. The air temperatures at the first several ejection holes near the channel entrance do not differ significantly from the inlet bulk temperature. Therefore, the relatively high velocities of the air flow through the ejection holes do not appear to affect the measurements of the static temperatures of the ejection airstream.

There is a small drop in the ejection airstream temperature at the last several ejection holes near the straight-flow exit in all runs with the straight-flow exit open. Since the local pressure in the pin fin channel is about the same as the atmospheric pressure near the straight-flow exit, there is almost no air flow through the last several ejection holes. The lower airstream temperatures at the exits of these ejection holes may be caused by the mixing of the air exiting the upstream ejection holes and the room air.

CONCLUDING REMARKS

Experiments have been conducted to study the heat transfer and friction characteristics of turbulent air flow through a pin fin channel with ejection holes. The following conclusions are drawn.

(1) When air exits through ejection holes, the heat transfer in the segments decreases much faster with increasing distance from the channel entrance than in the straight-flow-only case. The reduction in the mass flow rate in the pin fin channel lowers the heat transfer.

(2) Increasing the number of ejection holes and increasing the size of the ejection holes reduce the channel heat transfer and the overall channel pressure drop.

(3) In all ejection-flow cases, the distribution of the segmental heat transfer drops faster when Re_D is small than when Re_D is large.

(4) With no straight-flow exit, the channel heat transfer distribution drops faster with increasing distance from the channel entrance. Blocking the straight-flow exit also increases the overall channel pressure drop slightly.

(5) For straight flow through a pin fin channel, the segmental Nusselt number decreases slightly with increasing distance from the channel entrance. The Nusselt number can be predicted with a simple power function of the form $\bar{N}u_D = f(Re_D, n)$, where n is the segment number.

(6) The overall channel pressure drop is much higher in the straight-flow-only case than in any ejection-flow case.

Acknowledgement—This research was supported by the National Science Foundation (Grant No. CBT-8713833).

REFERENCES

1. A. Brown, R. Mandjikas and J. M. Mudyiwa, Blade trailing edge heat transfer. ASME Paper No. 80-GT-45 (1980).
2. G. J. VanFossen, Heat-transfer coefficients for staggered arrays of short pin fins, *ASME J. Engng Pwr* **104,** 268–274 (1982).
3. B. A. Brigham and G. J. VanFossen, Length to diameter ratio and row number effects in short pin fin heat transfer, *ASME J. Engng Gas Turbines Pwr* **106,** 241–245 (1984).
4. D. E. Metzger and S. W. Haley, Heat transfer experiments and flow visualization for arrays of short pin fins, ASME Paper No. 82-GT-138 (1982).
5. D. E. Metzger, R. A. Berry and J. P. Bronson, Developing heat transfer in rectangular ducts with staggered arrays of short pin fins, *ASME J. Heat Transfer* **104,** 700–706 (1982).
6. D. E. Metzger, W. B. Shepard and S. W. Haley, Row resolved heat transfer variations in pin-fin arrays including effects of nonuniform arrays and flow convergence, ASME Paper No. 86-GT-132 (1986).
7. S. C. Lau, Y. S. Kim and J. C. Han, Effects of pin configuration and entrance length on local endwall heat

mass transfer in a pin fin channel, ASME Paper No. 85-WA/HT-62 (1985).
8. S. C. Lau, J. C. Han and Y. S. Kim, Turbulent heat transfer and friction in pin fin channels with lateral flow ejection, *ASME J. Heat Transfer* **111,** 51–58 (1989).
9. S. C. Lau, J. C. Han and T. Batten, Heat transfer, pressure drop, and mass flow rate in pin fin channels with long and short trailing edge ejection holes, *ASME J. Turbomachinery* **111,** 116–123 (1989).
10. S. J. Kline and F. A. McClintock, Describing uncertainties in single-sample experiments, *Mech. Engng* **75,** 3–8 (1953).

TRANSFERT THERMIQUE SEGMENTAIRE DANS UN CANAL AVEC PICOTS ET TROUS D'EJECTION

Résumé—On étudie expérimentalement, pour l'écoulement turbulent d'air à travers un canal avec picots et trous d'éjection, les effets de la variation de la configuration des trous d'éjection sur la distribution du transfert thermique localement moyenné et la perte de pression globale. Le canal modélise les passages de refroidissement interne près du bord de fuite des ailettes de rotor et stator dans les turbines à gaz. Quand l'air sort par les trous d'éjection, le transfert de chaleur segmentaire diminue plus vite quand augmente la distance à l'entrée du canal et la perte de pression globale est plus faible que dans le cas de l'écoulement rectiligne. L'accroissement du nombre de trous d'éjection et de leur taille s'accompagne d'une diminution de la distribution du transfert thermique segmentaire et de la perte de pression globale.

WÄRMEÜBERGANG IN EINEM NADELRIPPENKANAL MIT AUSBLASEÖFFNUNGEN

Zusammenfassung—In der vorliegenden Arbeit wird bei turbulenter Luftströmung durch einen Nadelrippenkanal mit Ausblaseöffnungen der Einfluß der Anordnung dieser Öffnungen auf die Verteilung der regional gemittelten Wärmeübergangskoeffizienten und den Gesamtdruckabfall experimentell untersucht. Mit Hilfe dieses Kanals werden die inneren Kühlkanäle nahe der Abströmkante von Rotor- oder Statorschaufeln in modernen Gasturbinen nachgebildet. Wenn durch die Ausblaseöffnungen Luft austritt, vermindert sich der segmentgemittelte Wärmeübergang bei zunehmendem Abstand vom Kanaleintritt viel schneller und der Gesamtdruckabfall im Kanal ist geringer als im Fall der ungestörten Durchströmung. Mit zunehmender Anzahl und zunehmendem Durchmesser der Ausblaseöffnungen vermindern sich die Verteilung der segmentgemittelten Wärmeübergangskoeffizienten und der Gesamtdruckverlust.

ТЕПЛОПЕРЕНОС В СЕГМЕНТАХ КАНАЛА С ИГОЛЬЧАТЫМ ОРЕБРЕНИЕМ, ИМЕЮЩЕГО ОТВЕРСТИЯ ДЛЯ ВДУВА

Аннотация—Экспериментально исследовалось турбулентное течение воздуха по каналу с игольчатым оребрением, имеющему отверстия для вдува. Рассматривалось также влияние изменения конфигурации отверстий на распределение осредненного по участкам теплопереноса и суммарный перепад давления. Исследуемый канал моделировал каналы внутреннего охлаждения у задней кромки лопастей ротора или статора в современных двигателях газовых тубин. Когда воздух выходил через отверстия, теплоперенос в сегментах канала уменьшался намного быстрей с увеличением расстояния от входа в канал и суммарный перепад давления в канале был меньше, чем в случае только прямого течения. Увеличение количества отверстий для вдува и их размера приводило к выравниванию теплопереноса в сегмеитах канала и уменьшению суммарного перепада давления.